

Chapter 5:

Synthesis & Characterization of

Rare Earth Doped LaOF:

Investigation of Optical, Down

conversion and Upconversion

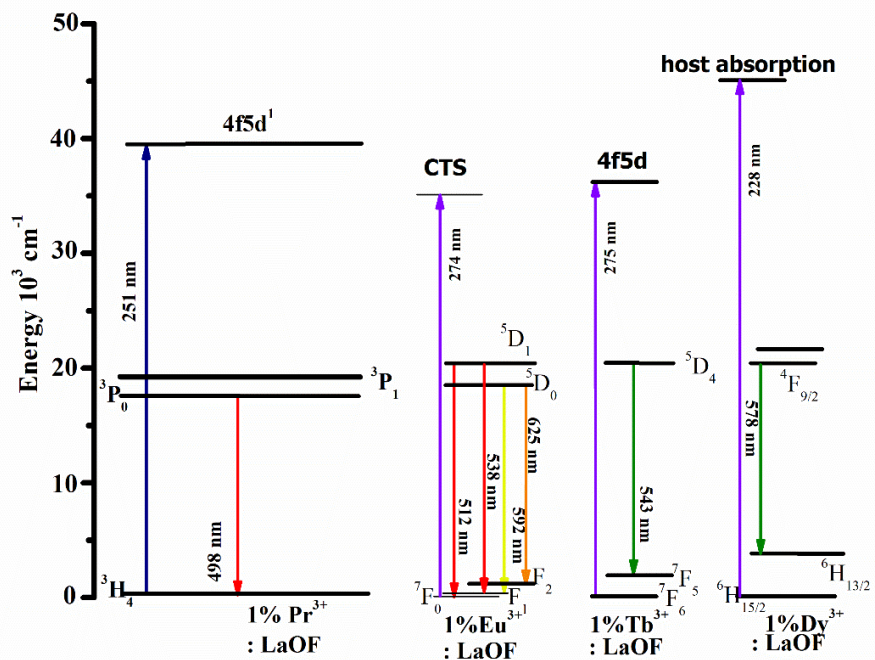
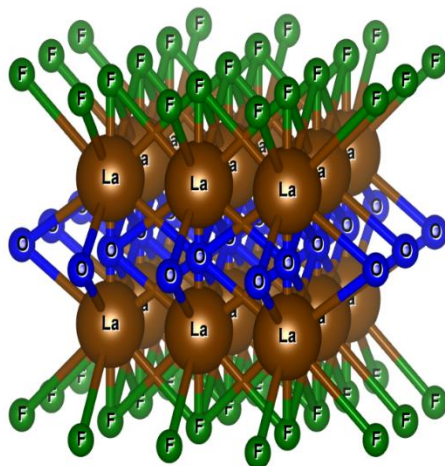
Properties

Abstract:

In this work, a simple route of synthesis for Nanoparticles (NP) of LaOF has been attempted. The Aegle marmelos gel (Bael leaves extract) assisted precipitation method was used to synthesize NP of undoped as well as doped LaOF. Four samples {Pr³⁺: LaOF, Eu³⁺: LaOF, Tb³⁺: LaOF, & Dy³⁺: LaOF} to study the down conversion properties and six samples {4% Yb³⁺ - 1% Er³⁺: LaOF, 12% Yb³⁺ - 2% Er³⁺: LaOF, 4% Yb³⁺ - 1% Ho³⁺: LaOF, 12% Yb³⁺ - 2% Ho³⁺: LaOF, 4% Yb³⁺ - 1% Tm³⁺: LaOF & 12% Yb³⁺ - 2% Tm³⁺: LaOF} to study the upconversion properties were synthesized by this technique. The Aegle marmelos gel acts as a biosurfactant that controls the particle growth. The structural, elemental, morphological, optical and photoluminescence characterization was carried out on synthesized samples. The XRD & EDAX analysis reveals that the obtained compounds possess high purity in the hexagonal phase and have crystallite size in nanometer. The optical bandgap and refractive index have been calculated from absorption characteristics obtained from UV – Visible spectra. From the SEM results, the average size of synthesized particles was found to be in the range of 34 nm to 88 nm with spherical shape.

Keyword: XRD, Aegle marmelos gel, UV-Visible analysis, PL analysis

Graphical abstract:



5.1 Introduction:

The morphology of materials is an important factor that affects the physical and chemical properties of the compounds. As the size of compounds or particles reduces to the Nanoscale, the particles' physical properties and chemical properties are greatly enhanced. This aspect has led to the rapid growth of nanotechnology. An appropriate synthesis technique has less complexity and gives high yield. It must be environment and industry friendly.

In this work, extract of Bael leaves, also known as *Aegle marmelos* gel-assisted precipitation method has been presented to synthesize nanoparticles of Lanthanum Oxyfluoride. The LaOF has remarkable applications in many scientific areas such as temperature sensing [1] [9], red-emitting phosphors [2], latent fingerprints sensor [3], solar cells [4], WLED phosphor [5], glass-ceramics [6], upconversion phosphor [7][8], biotechnology [10], anti-counterfeiting [11], thermal sensor [12], photocatalytic hydrogen production [13], etc.

These are several methods that have been reported previously for the synthesis of nanoparticles of LaOF, such as the sonochemical method [10][14], combustion synthesis technique [12][12][17], hydrothermal synthesis [13], solid-state technique [15], mechanochemical method [16], Aloe Vera based precipitation method [18], thermal decomposition method [19], stearic acid method [20], two-step hydrothermal method [21] and PITE assisted precipitation method [22].

In this work, pristine LaOF, four downconversion samples {1%Pr³⁺: LaOF, 1%Eu³⁺: LaOF, 1%Tb³⁺: LaOF, 1%Dy³⁺: LaOF} and six upconversion samples {4%Yb³⁺-1% Er³⁺: LaOF, 12%Yb³⁺-2% Er³⁺: LaOF, 4%Yb³⁺-1% Ho³⁺: LaOF, 12%Yb³⁺-2% Ho³⁺: LaOF, 4%Yb³⁺-1% Tm³⁺: LaOF and 12%Yb³⁺-2% Tm³⁺: LaOF} were synthesized by Bael leaves extract assisted precipitation method. The Bael extract, which is also known as *Aegle marmelos* gel was

prepared from fresh Bael leaves. In the synthesis process, the Aegle marmelos acts as biosurfactants that helps minimize the growth of LaOF particles. Thus reduces the particle size.

The Bael tree is considered to be sacred in Indian culture. The medical application of these Bael leaves is described in Rigveda, which is written over a thousand years ago.

5.2 Experimental Procedure:

One sample of pristine LaOF, four samples of down conversion phosphors {1% Pr³⁺: LaOF, 1% Eu³⁺: LaOF, 1% Tb³⁺: LaOF, 1% Dy³⁺: LaOF} and six samples of up-conversion phosphors {4% Yb³⁺ - 1% Er³⁺: LaOF, 12% Yb³⁺ - 2% Er³⁺: LaOF, 4% Yb³⁺ - 1% Ho³⁺: LaOF, 12% Yb³⁺ - 2% Ho³⁺: LaOF, 4% Yb³⁺ - 1% Tm³⁺: LaOF, 12% Yb³⁺ - 2% Tm³⁺: LaOF} were synthesized by modified precipitation synthesis technique.

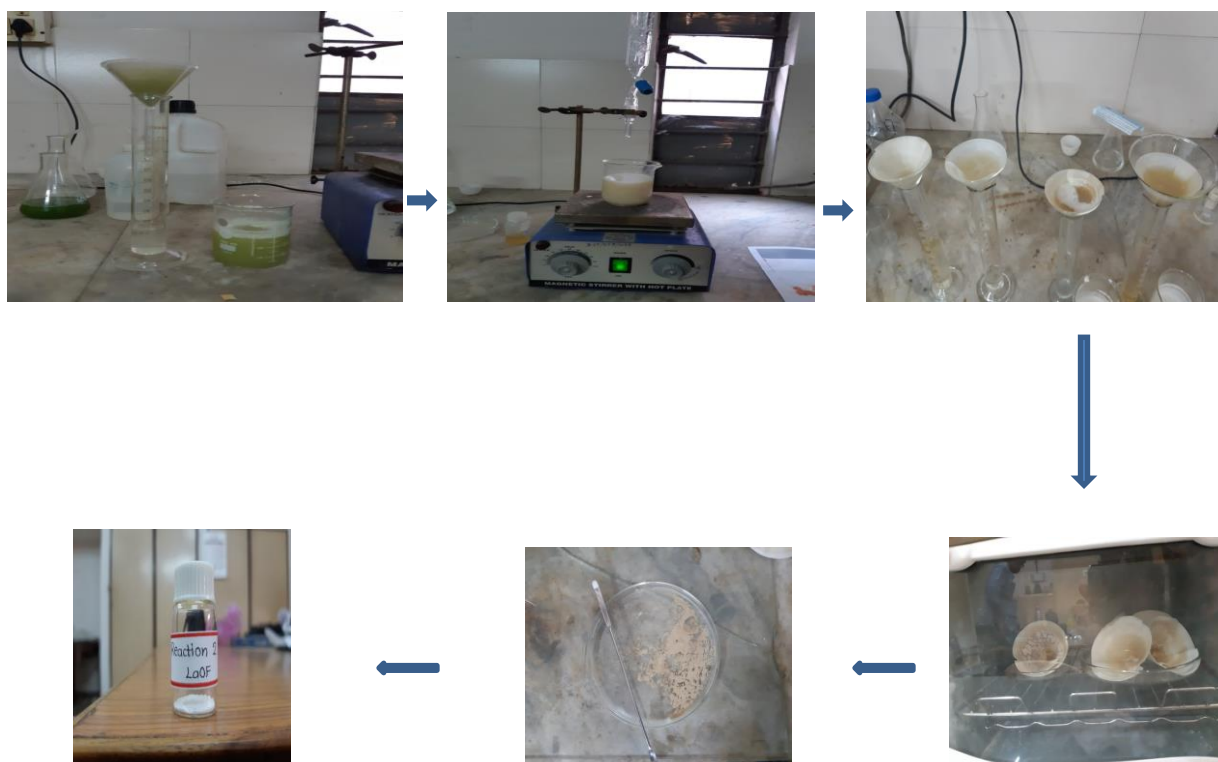
In the synthesis process of pristine LaOF, stoichiometric amount of La(NO₃)₃·6H₂O and NH₄F was dissolved in 100 ml De-ionized (DI) water and 20 ml of Bael leaf (Aegel Marmelous) extract was mixed with it.

For Bael leaf extract, a known amount (5gm) of freshly collected, taxonomically authenticated healthy leaves of Bael were washed thoroughly in tap water in the laboratory for 10 min in order to remove the dust particles and rinsed briefly in sterile distilled water. The leaves were dried naturally and crushed into powder using mortar and pestle. 200 ml water was added into the grinded powder of Bael leaves and the solution was heated at constant temperature of 70°C. The aqueous extract was cooled to room temperature and filtered through Whatman filter paper.



The mixture [$\text{La}(\text{NO}_3)_3 \cdot 6\text{H}_2\text{O}$ plus NH_4F plus 100 ml De-ionized (DI) water plus 20 ml of Aegel Marmelous] was poured into the borosil flask and continuously stirred on the magnetic stirrer for 2 hours at room temperature and the pH value was checked at regular intervals. As the pH value reached 3, the heat was applied to the solution to attain at a constant temperature of 50°C . NaOH solution was added drop by drop to turn the mixture acidic to neutral. The generation of precipitates starts on adding NaOH. The residues were filtered using Whatman filter paper. The residues were put in the oven at a constant temperature of 70°C . The obtained particles were crushed into the powder form with the help of mortar and pastel. The same procedure was applied for the synthesis of four down-conversion samples and six up-conversion samples.

The XRD, UV – Visible, SEM - EDAX & Photoluminescence studies were carried out to analyze their structural, morphological, optical & photoluminescence properties.



5.3 Results and Analysis of down conversion samples:

5.3.1 Structural, Morphological and Elemental analysis:

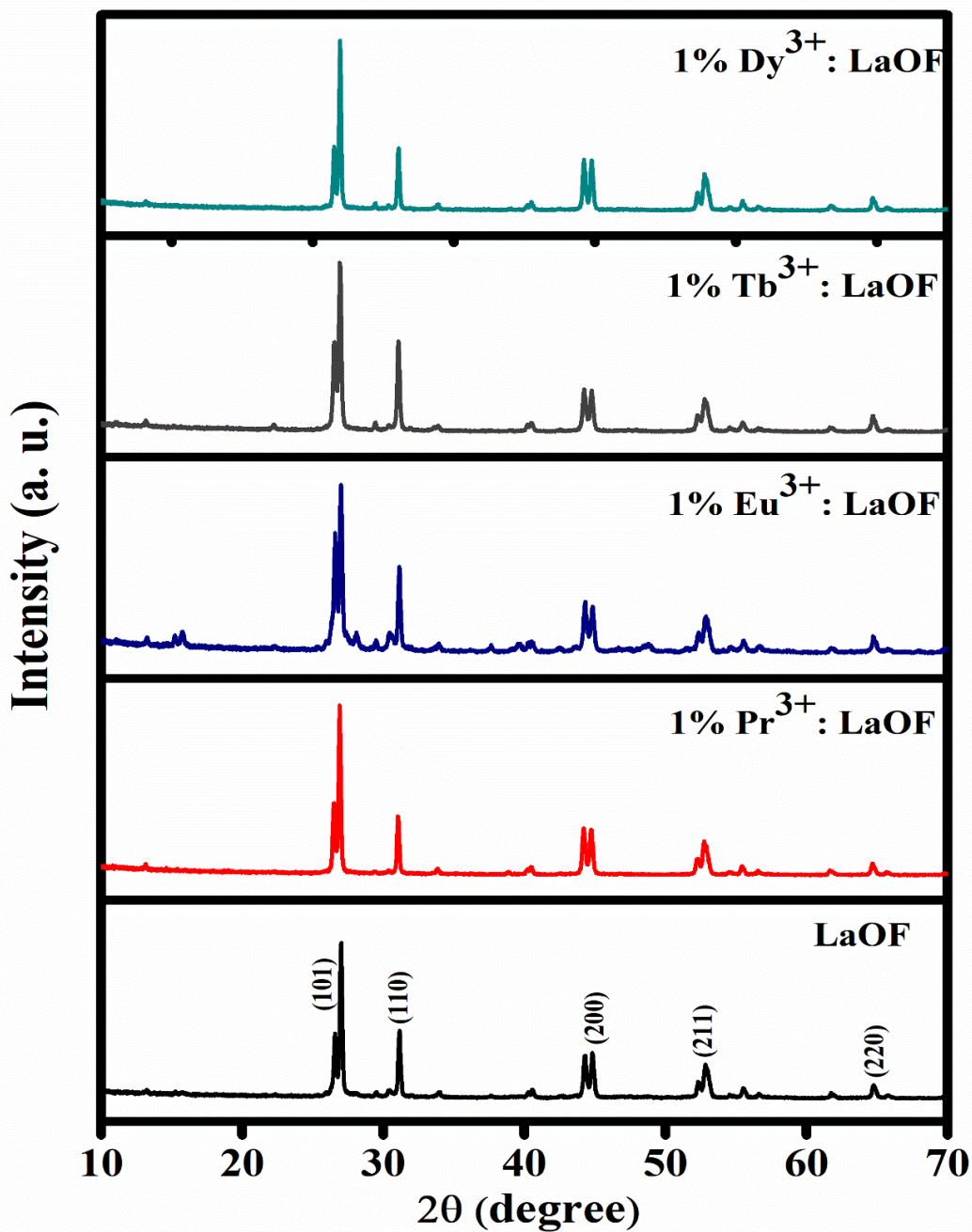


Figure 5.1 XRD of pristine and doped LaOF

Synthesized	Phase Name with	Matching Jcpds file	Avg. Crystallite	Lattice Parameters (Å ^o)	Volume (Å ^o) ³
-------------	-----------------	---------------------	------------------	--------------------------------------	---------------------------------------

Materials	Space Group	no.	Size (nm)	a	b	c	
LaOF	Tetragonal P 4/ n m m	89-5168	18.44	4.09	4.09	5.85	98.064
1% Pr ³⁺ : LaOF			18.19				
1% Eu ³⁺ : LaOF			17.43				
1% Tb ³⁺ : LaOF			16.02				
1% Dy ³⁺ : LaOF			15.45				

Table 5.1 Structural data of doped LaOF samples extracted from the XRD spectra

A Rigaku smartlab diffractometer operating at 30 mA, 40 kV with Cu K α radiation in the 2 θ range from 10 to 90 $^\circ$, with the step of 0.02 $^\circ$ was used for XRD characterization. Figure 5.1 shows the XRD spectrum of pristine LaOF along with four samples of down conversion phosphors {1% Pr³⁺: LaOF, 1% Eu³⁺: LaOF, 1% Tb³⁺: LaOF, 1% Dy³⁺: LaOF}. The structural data from the XRD pattern (fig. 5.1) is given in table 5.1. The peaks match with the JCPDS files no. 89-5168. All the samples have tetragonal structure with space group P 4/n m m. The highest peaks are observed at 2 θ values of 26 $^\circ$ 19' with the hkl plan (1 0 1) in all samples. The crystallite size estimated by the Scherrer equation shows a small decrease from pristine to doped samples. Since the pattern of the atomic radius is La>Pr>Eu>Tb>Dy, all rare-earth dopant elements have an ionic radius less than the host element Lanthanum. This is the likely reason behind the decrease in crystallite size.

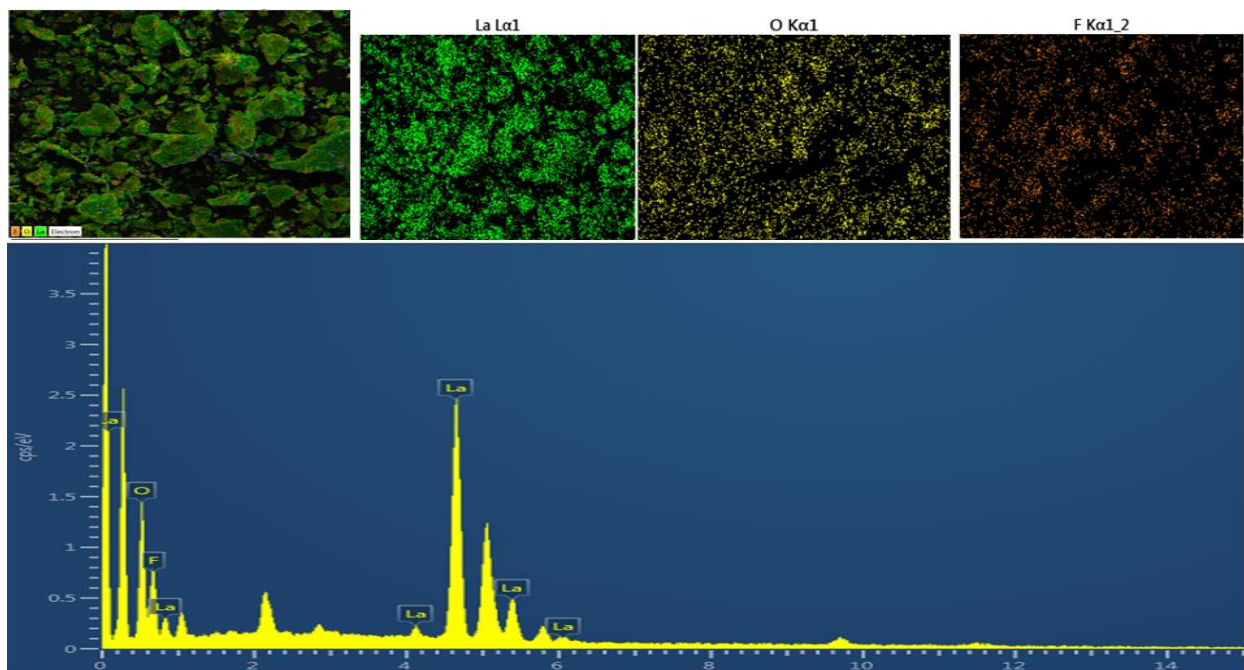


Figure 5.2 (a) EDAX Spectrum with mapping of LaOF

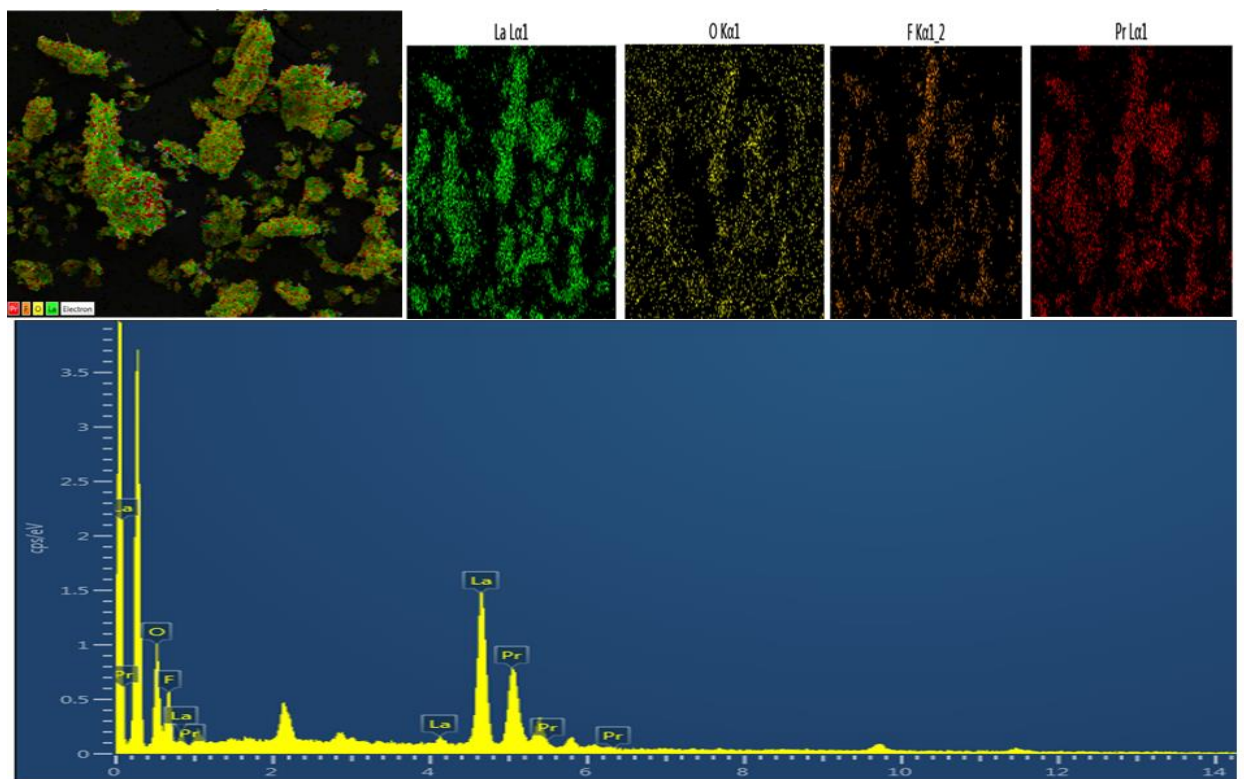


Figure 5.2 (b) EDAX Spectrum with mapping of 1% Pr³⁺: LaOF

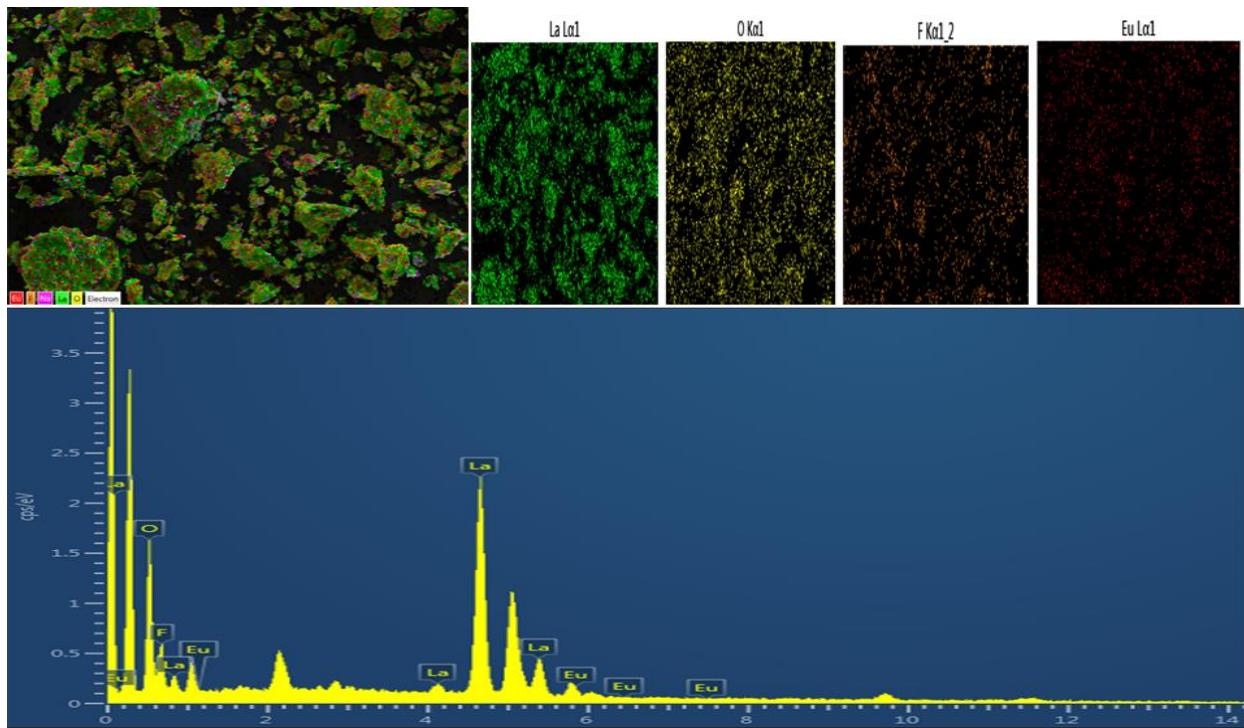


Figure 5.2 (c) EDAX Spectrum with mapping of 1% Eu^{3+} : LaOF

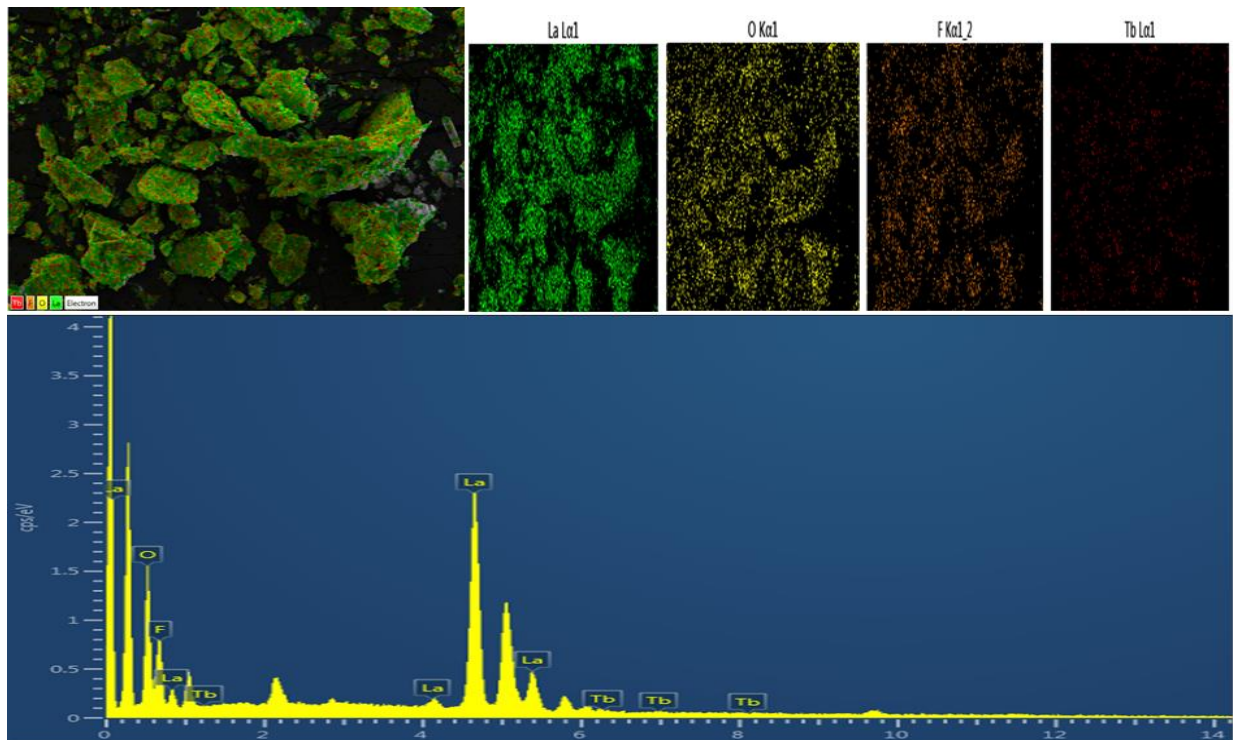


Figure 5.2 (d) EDAX Spectrum with mapping of 1% Tb^{3+} : LaOF

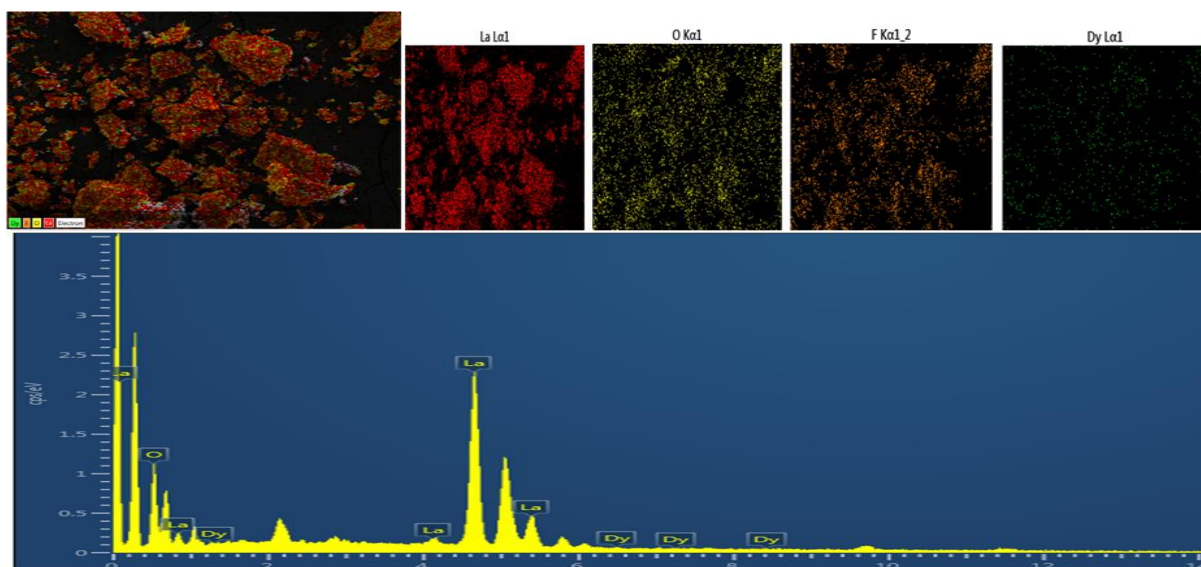


Figure 5.2 (e) EDAX Spectrum with mapping of 1% Dy³⁺: LaOF

Compounds	Elements (Atomic %)						
	La	O	F	Pr	Eu	Tb	Dy
LaOF	39.2	28.6	32.2	-	-	-	-
LaOF: Pr ³⁺	38.5	28.9	32.3	0.3	-	-	-
LaOF: Eu ³⁺	36.5	30.9	32.3	-	0.3	-	-
LaOF: Tb ³⁺	35.5	31.9	32.3	-	-	0.3	-
LaOF: Dy ³⁺	33.5	32.9	33.3	-	-	-	0.3

Table 5.2 EDAX data of 1% Ln³⁺: LaOF from the spectrum with Atomic percentage

Fig. 5.2 (a to e) shows the EDAX Spectrum with mapping of LaOF and 1% Ln³⁺: LaOF. The spectrum shows traces of all lanthanide ions doped into the Lanthanum oxyfluoride and also identifies the elements of the samples. Table 5.2 shows the data extracted from the EDAX spectrum with an atomic percentage in composition.

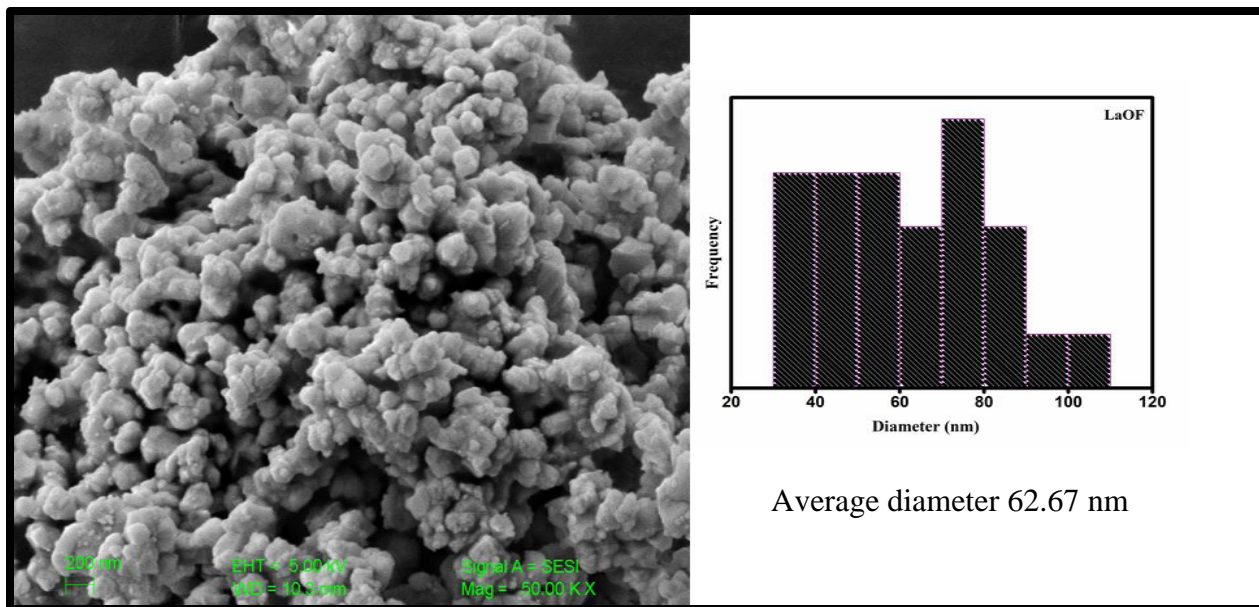


Figure 5.3 (a) SEM images with histogram of LaOF

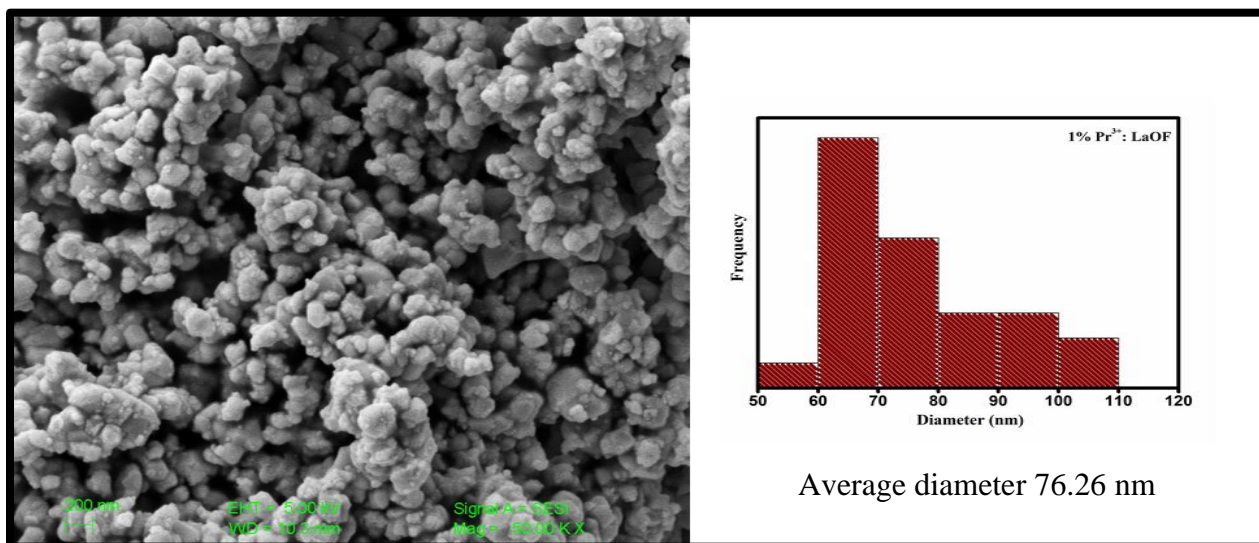


Figure 5.3 (b) SEM images with histogram of 1% Pr³⁺: LaOF

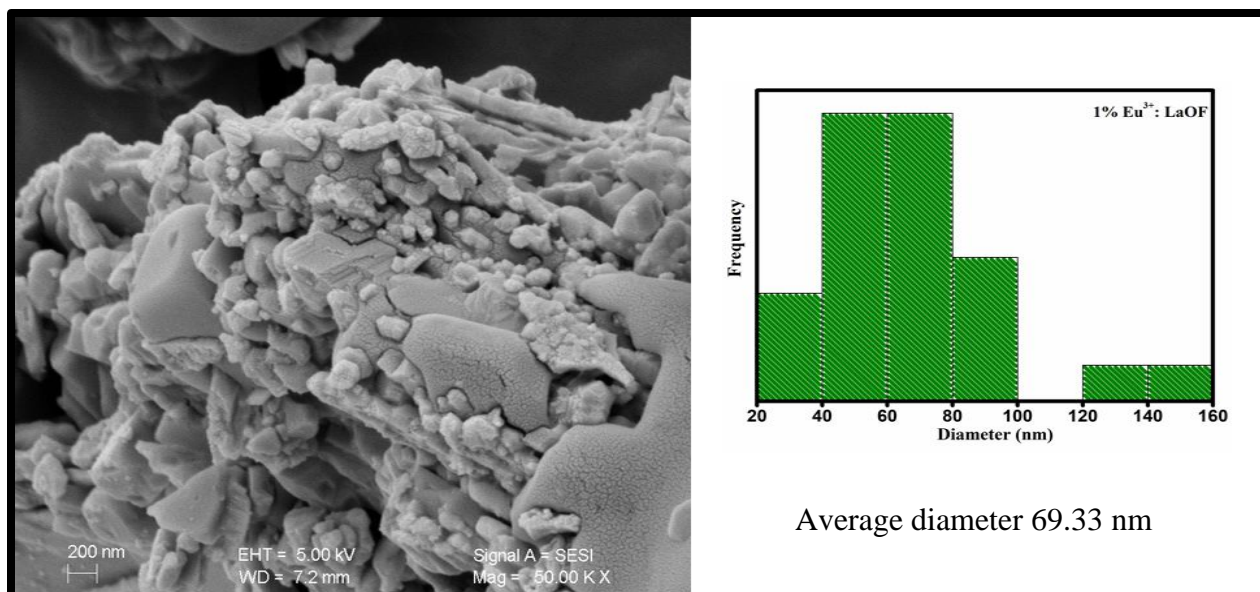


Figure 5.3 (c) SEM images with histogram of 1% Eu³⁺: LaOF

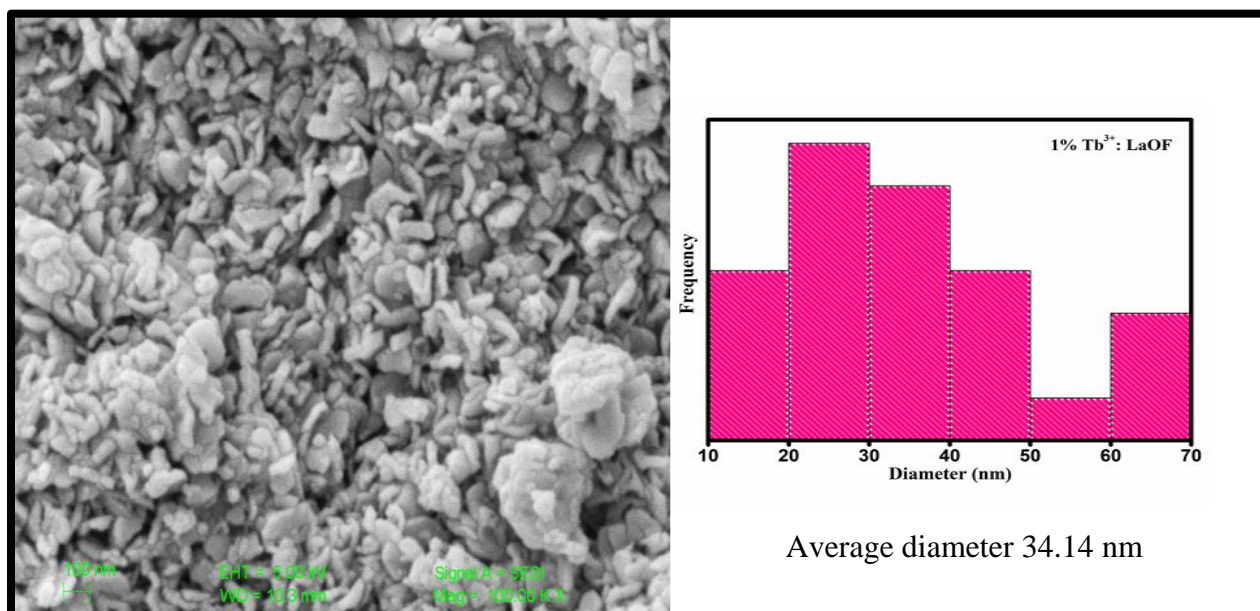


Figure 5.3 (d) SEM images with histogram of 1% Tb³⁺: LaOF

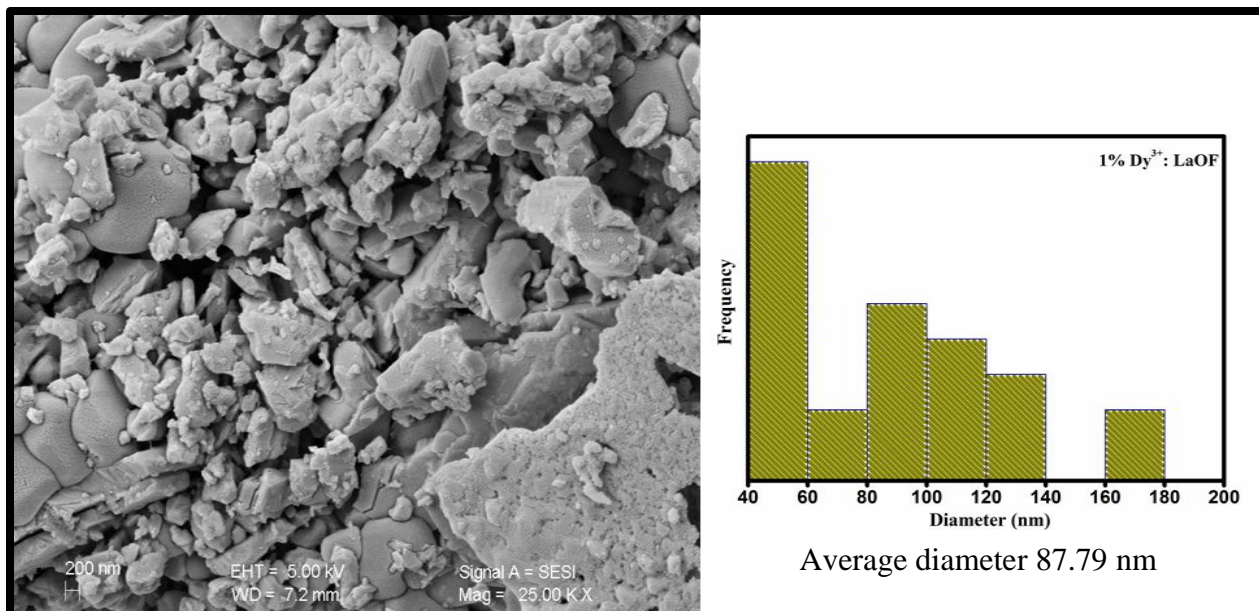


Figure 5.3 (e) SEM images with histogram of 1% Dy³⁺: LaOF

Fig. 5.3 represents the SEM images of Ln³⁺: LaOF with histogram of particle size distribution. The average particle size was found to be in the range of 34 nm to 88 nm. The morphology was found to be spherical in some samples.

5.3.2 UV – Visible analysis:

Shimadzu spectrometer was used for UV-Visible characterization of the samples. A 0.05 M aqueous solution was used for the purpose.

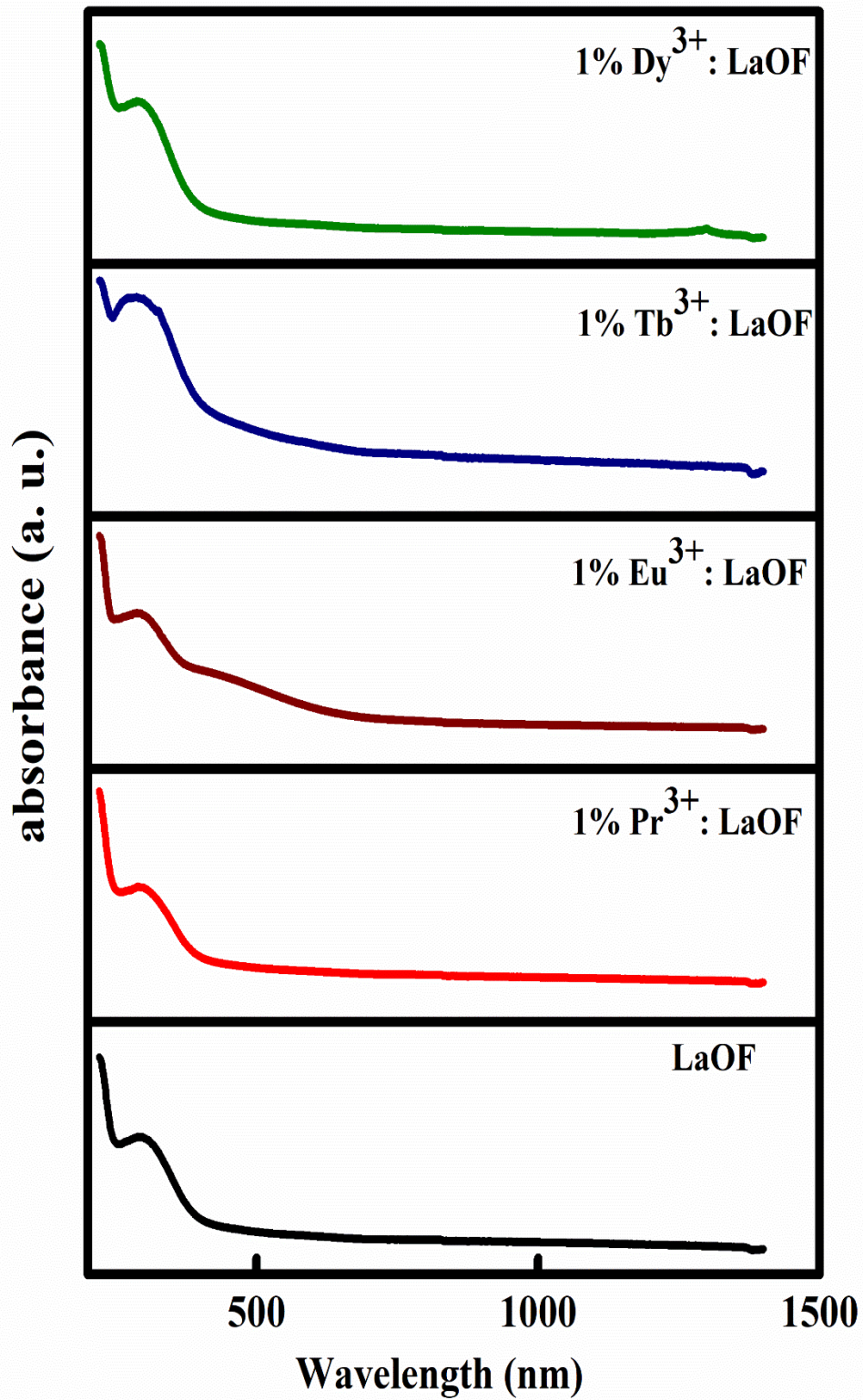


Figure 5.4 UV-Visible characteristics of 1% Ln³⁺: LaOF

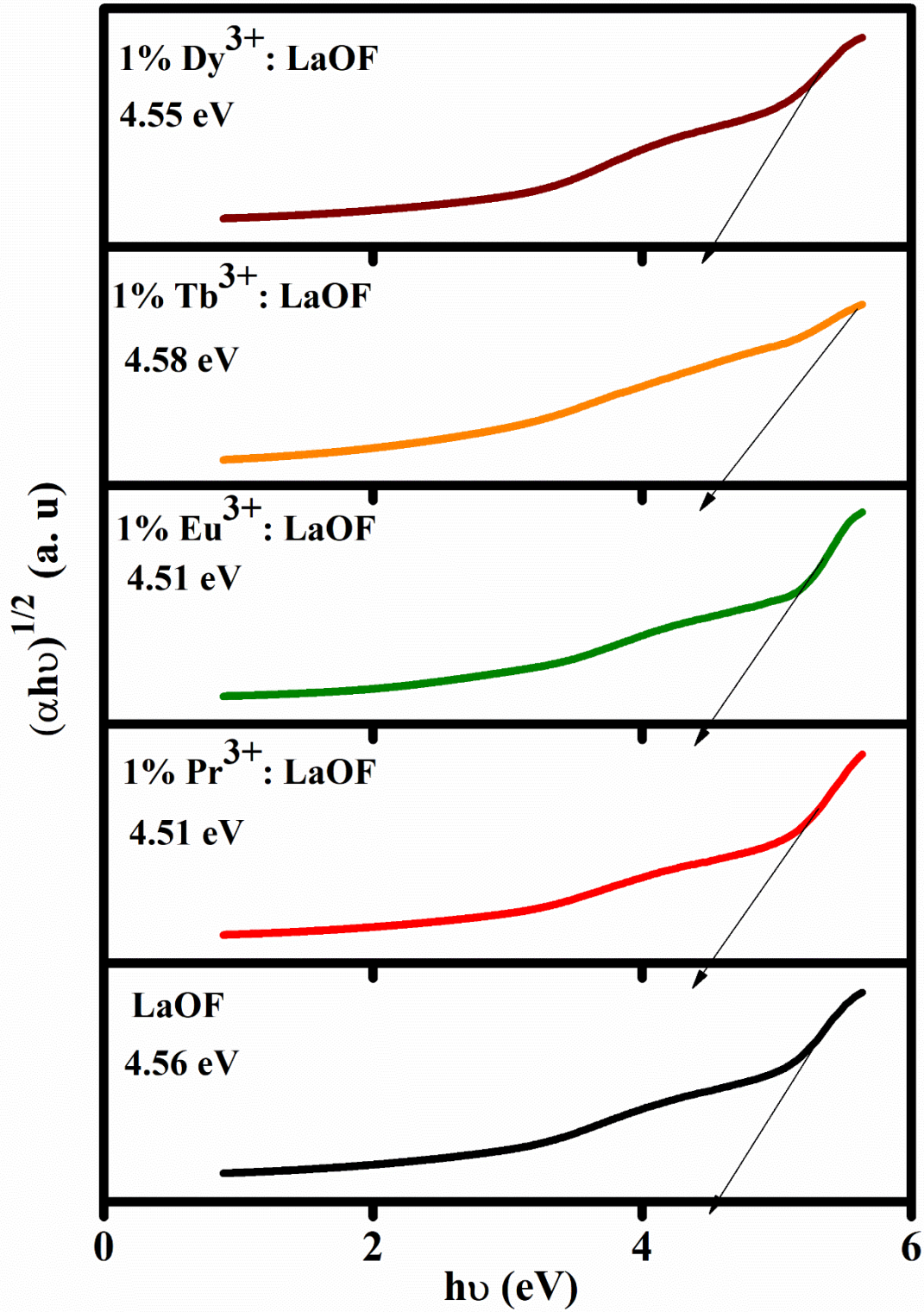


Figure 5.5 Tauc's plot for samples

Compounds	λ_{\max} (nm)	Band Gap (eV)	Refractive index η
LaOF	295	4.56	2.06
1% Pr ³⁺ : LaOF	290	4.51	2.07
1% Eu ³⁺ : LaOF	290	4.51	2.07
1% Tb ³⁺ : LaOF	282	4.58	2.06
1% Dy ³⁺ : LaOF	286	4.55	2.06

Table 5.3 UV/VIS data of host LaOF as well as 1% Ln³⁺: LaOF

Fig 5.4 shows the absorbance graph of pristine LaOF and four samples of 1%Ln³⁺: LaOF. Fig 5.5 shows the Tauc's plot for the calculation of optical band gap. Table 5.3 gives the data of the wavelength at which maximum absorbance takes place, the optical bandgap and the refractive index. From the fig 5.4, the maximum absorbance peaks are observed at the wavelength between 282 nm to 295 nm. The possible reason for this is the absorption between 2p orbital of O⁻² to 4f orbital of Ln³⁺.

For the optical band calculation, Tauc's plot was used [23]. The graph was plotted between $(\alpha h\nu)^{1/n} \rightarrow (h\nu)$ gives the optical band gap value. Here $n = 2$ taken for the allowed indirect electronic transition. The refractive index η was also calculated [24].

5.3.3 Photoluminescence analysis:

The Photoluminescence excitation and emission spectra were recorded on a Shimadzu make Spectrophotofluorometer.

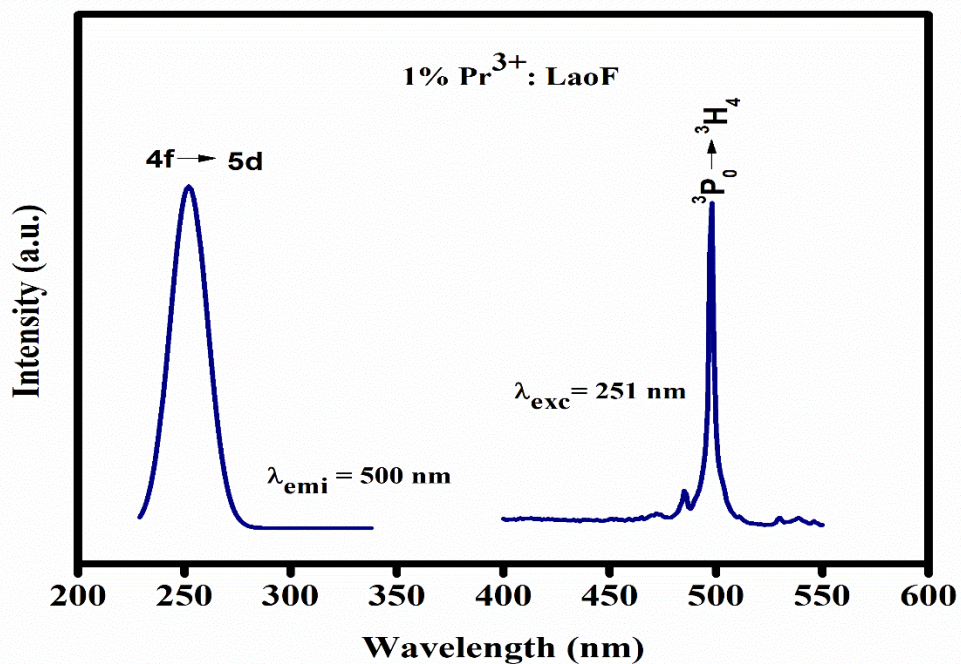


Figure 5.6 (a) Excitation and Emission spectra of 1%Pr³⁺: LaOF

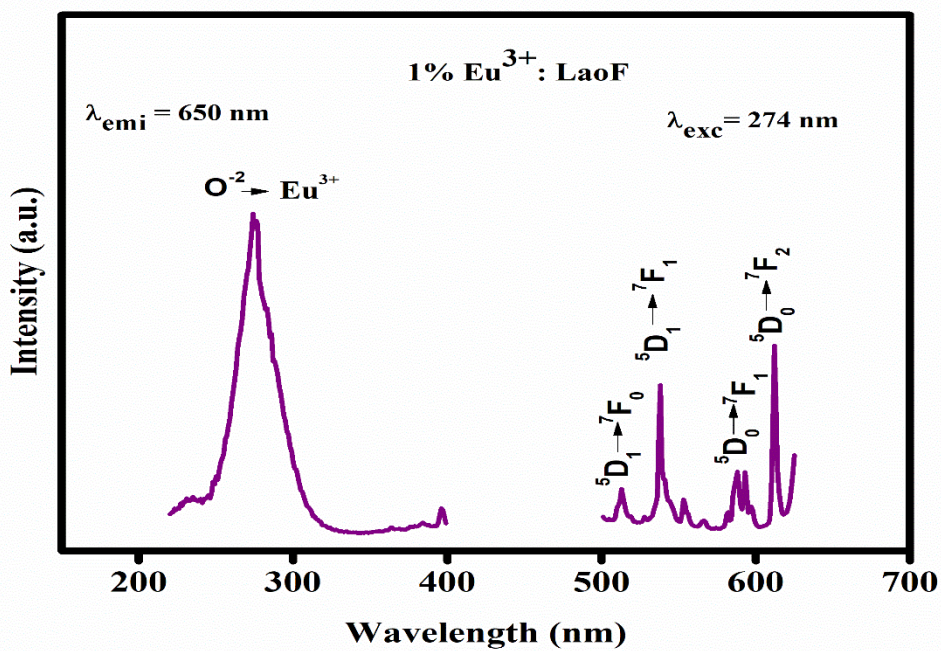


Figure 5.6 (b) Excitation and Emission spectra of 1%Eu³⁺: LaOF

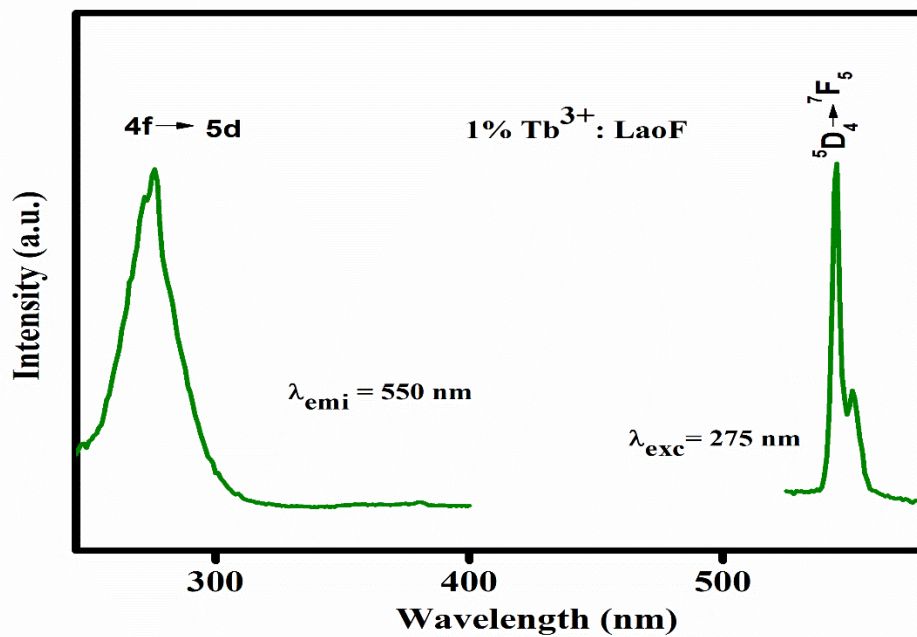


Figure 5.6 (c) Excitation and Emission spectra of 1% Tb³⁺: LaOF

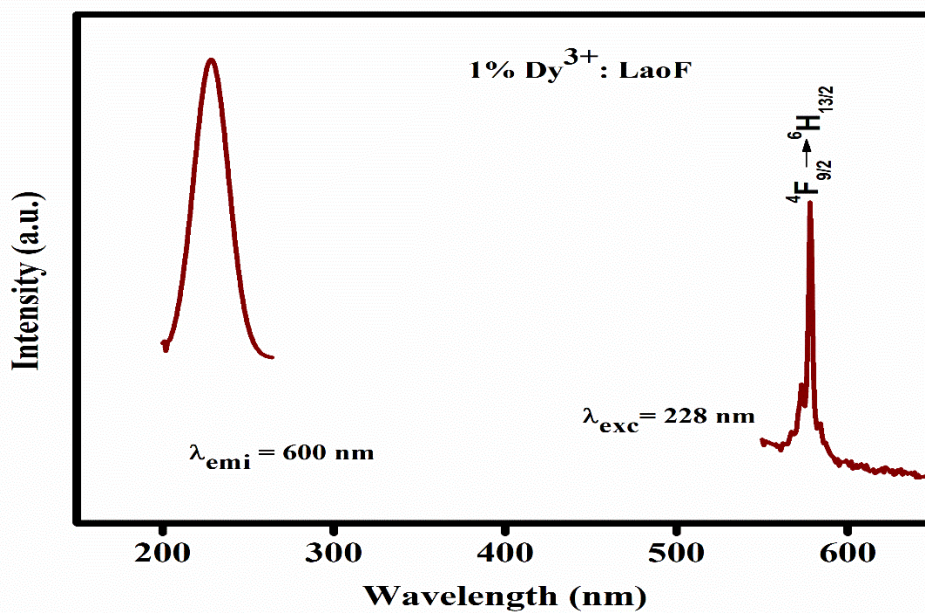


Figure 5.6 (d) Excitation and Emission spectra of 1% Dy³⁺: LaOF

PL excitation and emission spectra of Pr³⁺: LaOF is shown in fig. 5.6 (a). The excitation spectra was recorded at the emission wavelength of $\lambda_{\text{emi}} = 500$ nm. The 4f5d transition in Pr³⁺: LaOF is responsible for the excitation band with a maximum wavelength of 251 nm. The emission spectra was recorded at the excitation wavelength of $\lambda_{\text{emi}} = 251$ nm. There is only one intense and sharp emission peak observed at 498 nm. The transition from ³P₀ to ground energy level ³H₄, is responsible for this peak[25].

From the fig 5.6 (b) for Eu³⁺: LaOF, PL excitation peak is observed at 274 nm for the emission wavelength $\lambda_{\text{emi}} = 650$ nm. The CTS (charge transfer stage) transition is accountable for PL excitation spectra for Eu³⁺: LaOF in which transition between 2p orbital of O²⁻ and 4f orbital of Eu³⁺ occurs. The emission spectrum was recorded at an excitation wavelength of $\lambda_{\text{exc}} = 274$ nm. There are eight emission peaks, spotted at wavelengths of 512 nm, 538 nm, 555 nm, 587 nm, 592 nm, 597 nm, 612 nm and 625 nm. All are due to 4f-4f the transition. The specific transitions are; ⁵D₁ to ⁷F₀ for emission at 512 nm; ⁵D₁ to ⁷F₁ for 538 nm & 555 nm; ⁵D₀→⁷F₁ for 587 nm, 590 nm and 597 nm; ⁵D₀ →⁷F₂ for emission at 612 nm and 625 nm[25].

From fig 5.6 (c) for Tb³⁺: LaOF, the maximum excitation is observed at a wavelength of 275 nm under the emission wavelength λ_{emi} of 550 nm. The 4f5d transition in Tb³⁺: LaOF is accountable for the excitation spectra. Under the excitation of 275 nm, only one strong emission peak is observed. The transition ⁵D₄→⁷F₅ is responsible for this intense peak at 550 nm [25].

From fig 5.6 (d) for Dy³⁺: LaOF, the excitation spectrum was recorded at an emission wavelength of 600 nm. The excitation was maximum at a wavelength of 228 nm. The host absorption is accountable for excitation in 1% Dy³⁺: LaOF. Under the excitation at a wavelength of 228 nm, the highest intensity emission peak was recorded at 578 nm, which is due to the ⁴F_{9/2} → ⁶H_{13/2} transition [25].

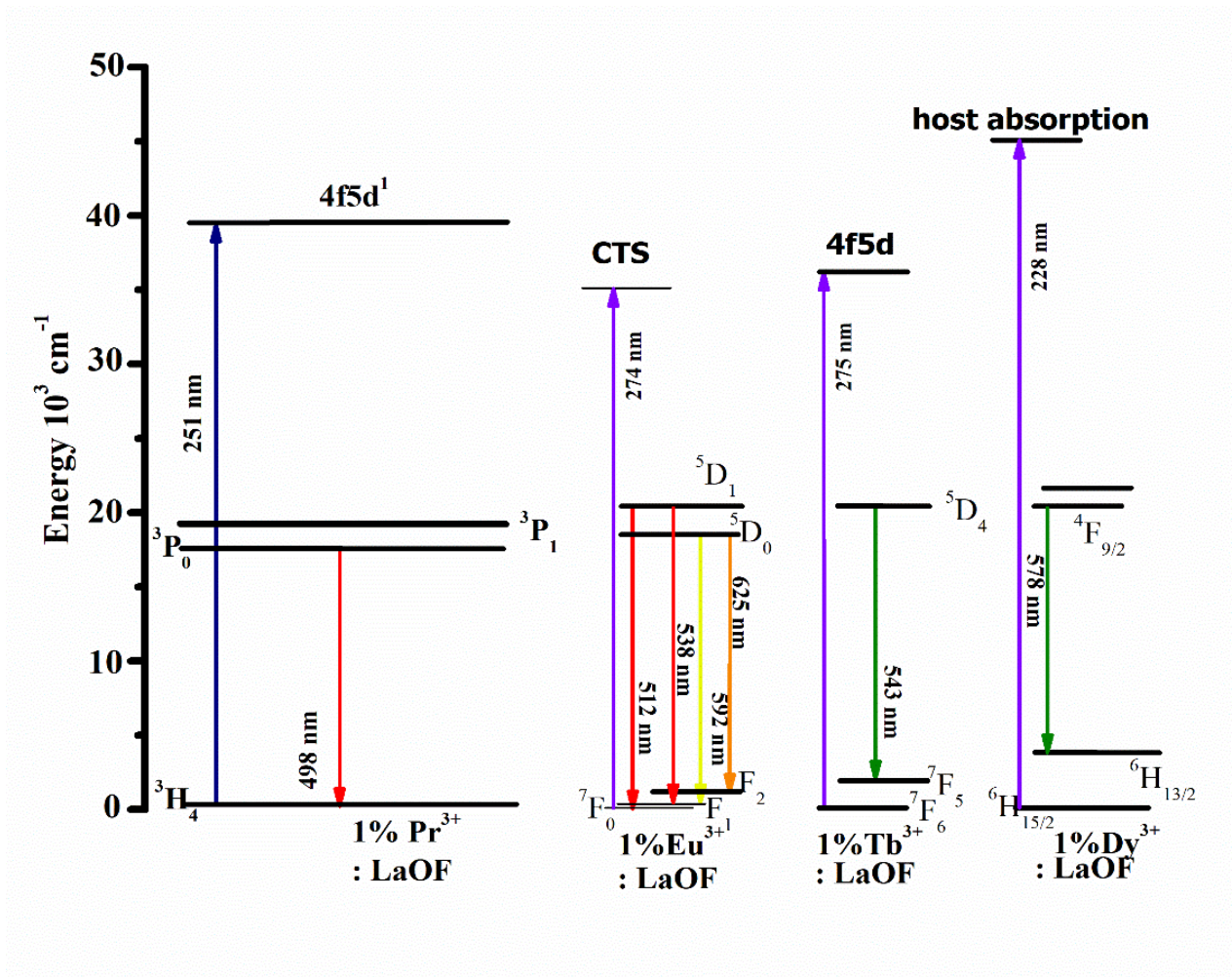


Figure 5.7 Energy level diagram for down conversion photoluminescence

5.4 Results and Analysis for upconversion samples:

5.4.1 Structural analysis:

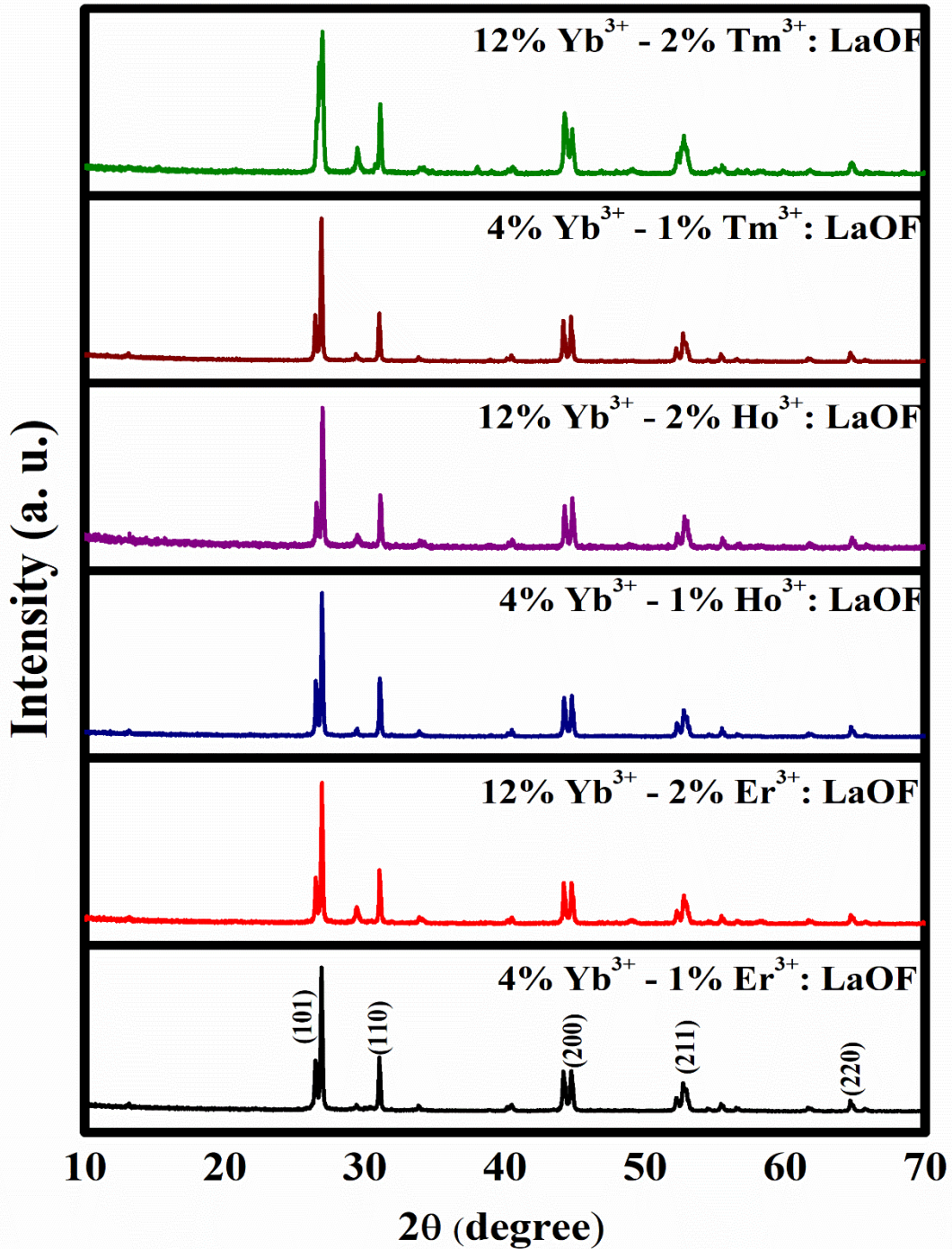


Figure 5.8 XRD of upconversion samples

Synthesized Materials	Phase Name with Space Group	Matching Jcpds file no.	Avg. Crystallite Size (nm)	Lattice Parameters (Å°)			Volume (Å°) ³
				a	b	c	
4% Yb ³⁺ - 1% Er ³⁺ : LaOF	Tetragonal P 4/ n m m	89-5168	15.21	4.09	4.09	5.85	98.064
12% Yb ³⁺ - 2% Er ³⁺ : LaOF			14.11				
4% Yb ³⁺ - 1% Ho ³⁺ : LaOF			13.77				
12% Yb ³⁺ - 2% Ho ³⁺ : LaOF			12.16				
4% Yb ³⁺ - 1% Tm ³⁺ : LaOF			11.64				
12% Yb ³⁺ - 2% Tm ³⁺ : LaOF			10.12				

Table 5.4 Structural data of doped La₂O₃ samples extracted from the XRD spectra

5.4.2 Upconversion Photoluminescence analysis:

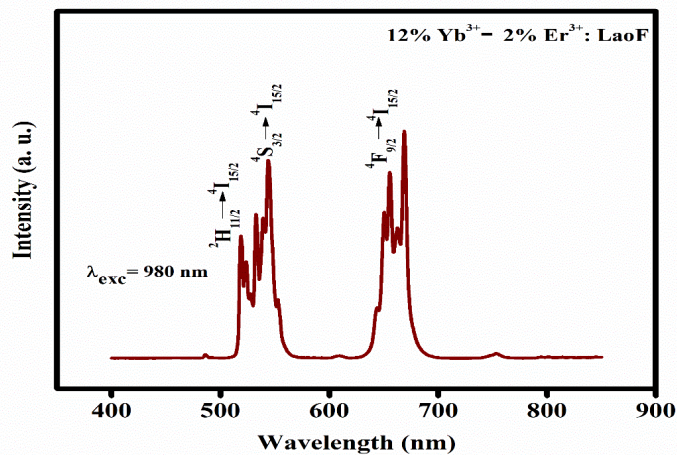


Figure 5.9 (a) Emission characteristics of 12%Yb³⁺-2%Er³⁺: LaOF

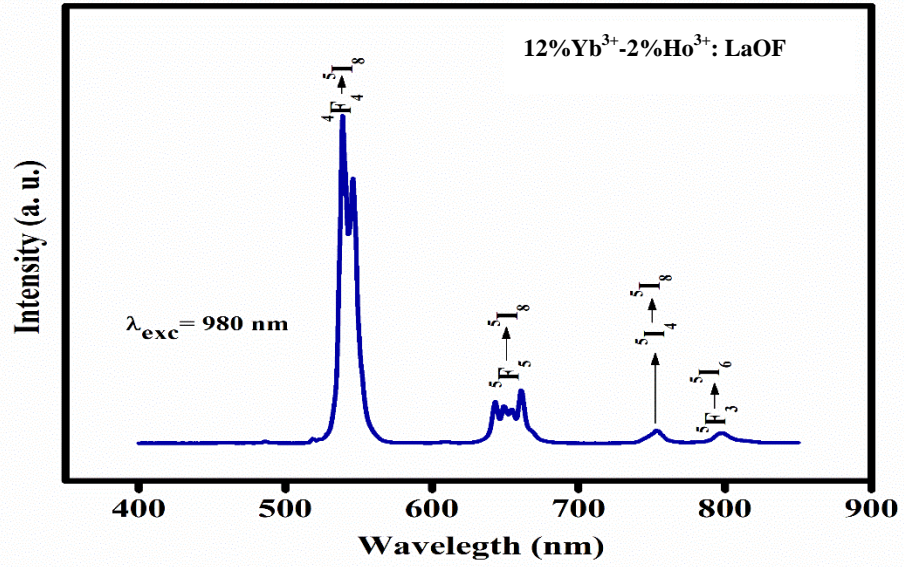


Figure 5.9 (b) Emission characteristics of 12%Yb³⁺-2%Ho³⁺: LaOF

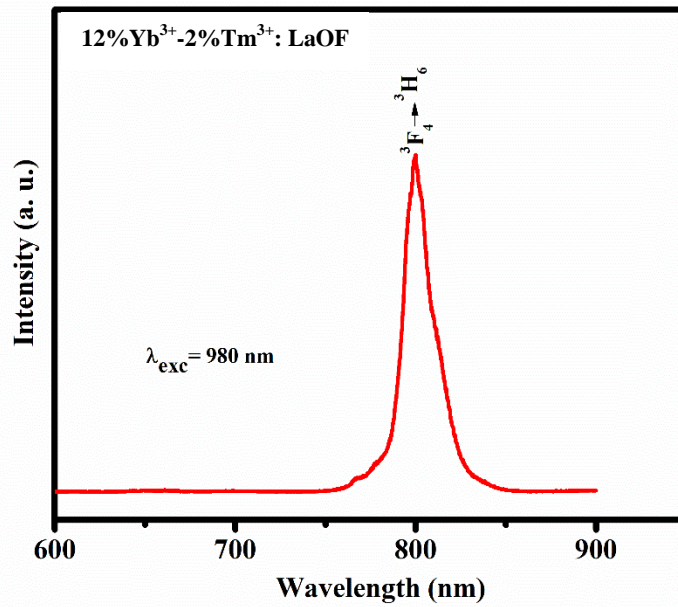


Figure 5.9 (c) Emission characteristics of 12%Yb³⁺-2%Tm³⁺: LaOF

For Upconversion Photoluminescence, the emission was recorded on the fiber-optic coupled high-resolution spectrograph (Horiba Jobin-Yvon make FHR 1000 model with ICCD detector). Only three samples give upconversion photoluminescence.

The PL upconversion spectrum given in fig 5.9 (a) for 12% Yb³⁺- 2%Er³⁺: LaOF was recorded under 980 nm excitation. Five peaks were observed at 519 nm, 532 nm, 543 nm, 655 nm and 670 nm. The emission at 519 nm is due to the transition from ²H_{11/2} to ⁴I_{15/2}, emission at 532 nm & 543 nm due to the ⁴S_{3/2} to ⁴I_{15/2} transition and emission at 655 nm & 670 nm due to ⁴F_{9/2}→⁴I_{15/2} transition [25].

From fig 5.9 (b) for 12% Yb³⁺- 2%Ho³⁺: LaOF was also recorded under 980 nm excitation. Here also, five peaks were observed at 538 nm, 643 nm, 662 nm, 754 nm and 800 nm. The emission at 538 nm is due to the transition from ⁴F₄ to ⁵I₈, emission at 643 nm & 662 nm is due to the transition from ⁵F₅ to ⁵I₈, emission at 754 nm is due to the transition from ⁵I₄ to ⁵I₈ & 800 nm due to ⁵F₃→⁵I₆ transition [25].

From fig 5.9 (c) for 12% Yb³⁺- 2%Tm³⁺: LaOF for the same excitation, the emission at wavelength of 800 nm is due to the ³F₄→³H₆ transitions [25].

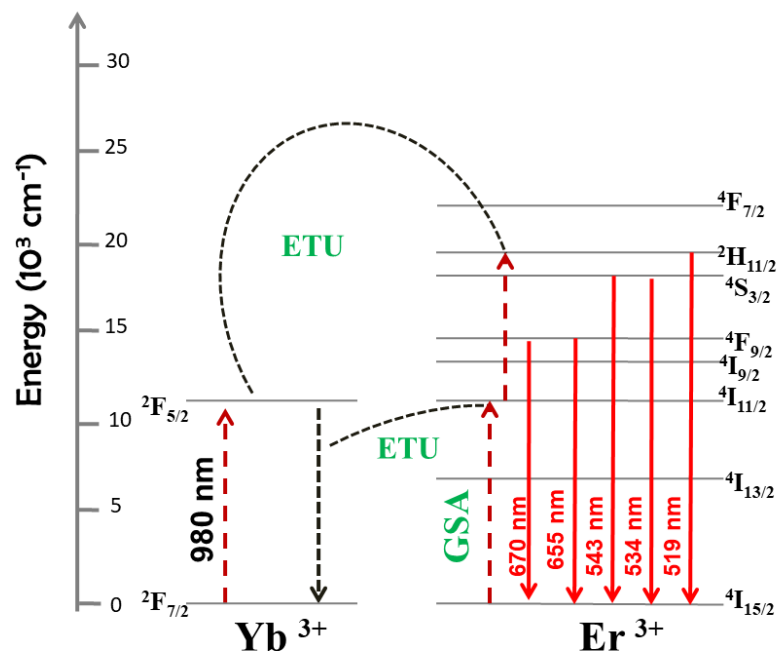


Figure 5.10 (a) Energy level diagram for Upconversion photoluminescence of 12% Yb³⁺-2% Er³⁺: LaOF

As shown in fig. 5.10 (a), the excitation energy at 980 nm is absorbed by the Yb³⁺ as well as Er³⁺ ions. The Yb³⁺ ions and Er³⁺ ions have the same energy for the first excited state. The excitation results into transitions from ${}^2F_{7/2} \rightarrow {}^2F_{5/2}$ levels in Yb³⁺ ions and ${}^4I_{15/2} \rightarrow {}^4I_{11/2}$ levels in Er³⁺ ions. Thus both the ions undergo Ground State Absorption. The energy emitted by the Yb³⁺ ions while returning to the ground state is transferred to the Er³⁺ ions, due to which they are propelled to the higher energy levels as shown in the diagram. The decay from these higher energy levels to the ground state ${}^4I_{15/2}$ in Er³⁺ ions results in emissions.

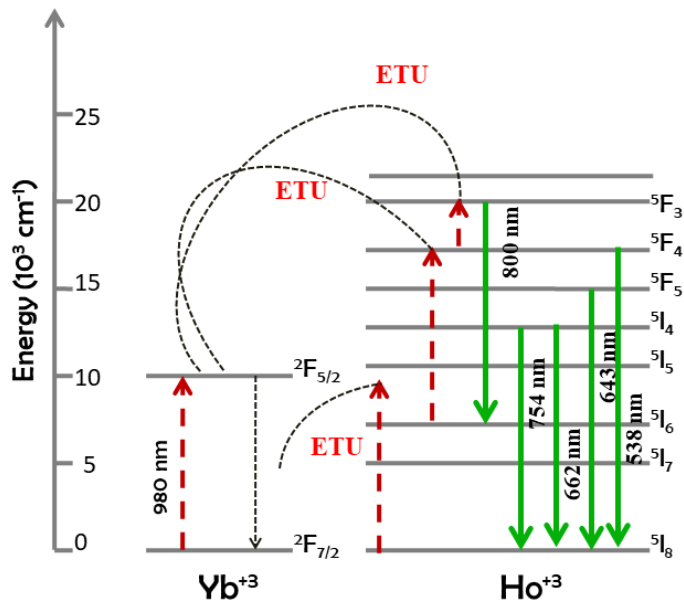


Figure 5.10 (b) Energy level diagram for Upconversion photoluminescence of 12% Yb³⁺-2% Ho³⁺: LaOF

As shown in fig 5.10 (b) for 12% Yb³⁺- 2% Ho³⁺: LaOF, the excitation at 980 nm is absorbed by only Yb³⁺ ions. This ground state absorption results into the transition $^2F_{7/2} \rightarrow ^2F_{5/2}$ and subsequent emission from $^2F_{5/2} \rightarrow ^2F_{7/2}$. The emitted energy also triggers the ground state absorption of Ho³⁺ ions from 5I_8 . The emitted energy from Yb³⁺ ions further excites the Ho³⁺ ions at 5I_6 to the higher energy levels. The Ho³⁺ ions are further excited to the 5F_3 level via ETU. The decay to 5I_3 level results in emission in the IR region at 800 nm. The decay from these higher energy levels to the ground state 5I_8 in Ho³⁺ ions results in visible emissions.

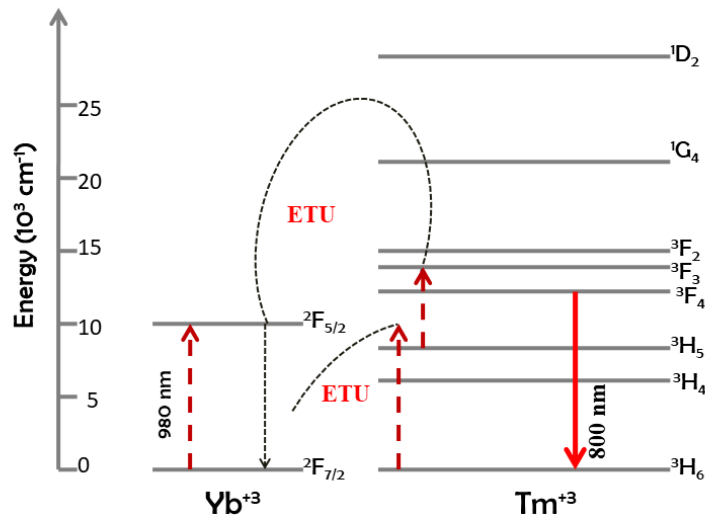


Figure 5.10 (c) Energy level diagram for Upconversion photoluminescence of 12% Yb³⁺-2% Tm³⁺: LaOF

As shown in fig 5.10 (c) for 12% Yb³⁺- 2% Tm³⁺: LaOF, the excitation at 980 nm is absorbed by only Yb³⁺ ions. This ground state absorption results into the transition ${}^2F_{7/2} \rightarrow {}^2F_{5/2}$ and subsequent emission from ${}^2F_{5/2} \rightarrow {}^2F_{7/2}$. The emitted energy triggers the ground state absorption of Tm³⁺ ions from 3H_6 . The emitted energy from Yb³⁺ ions further excites the Tm³⁺ ions at 3H_5 also to other excited states as shown in figure. The transition from excited states to the ground state 3H_6 of Tm³⁺ ions results in emissions.

5.5 Conclusion:

The nanoparticles of the pristine and doped Lanthanum Oxyfluoride were successfully synthesized by precipitation method using Bael leaf extract also known as Aegle marmelos gel as bio-surfactant. The structural, elemental and optical properties of obtained samples are studied using the XRD, EDAX, UV-Visible and Photoluminescence technique respectively. The average size of synthesized particles is in the range of 34 nm to 88 nm.

References:

- [1] H. Zhang, X. Dong, L. Jiang, Y. Yang, X. Cheng, H. Zhao, Comparative analysis of upconversion emission of LaF₃:Er/Yb and LaOF:Er/Yb for temperature sensing, *J. Mol. Struct.* 1206 (2020) 127665. doi:10.1016/j.molstruc.2019.127665.
- [2] S. Wang, Y. jie Han, L. Shi, W. yuan Zhang, P. mei Shi, Z. fei Mu, S.B. Shen, X.L. Lu, Z. wei Zhang, A. jun Song, Red-emitting LaOF:Eu³⁺ phosphor modified by tetraethyl orthosilicate to boost the Luminescence intensity for LEDs, *Optik (Stuttg)*. 223 (2020) 165574. doi:10.1016/j.ijleo.2020.165574.
- [3] C. Suresh, G.P. Darshan, S.C. Sharma, M. Venkataravanappa, H.B. Premkumar, S. Shanthi, K.N. Venkatachalaiah, H. Nagabhushana, Imaging sweat pore structures in latent fingerprints and unclonable anti-counterfeiting patterns by sensitizers blended LaOF:Pr³⁺ nanophosphors, *Opt. Mater. (Amst)*. 100 (2020) 109625.
- [4] Z. Shariatinia, Z. Zolfaghari-Isavandi, Application of Zn_xLa_yFe_zO₄ spinel nanomaterial in quantum dot sensitized solar cells, *Optik (Stuttg)*. 212 (2020) 164682. doi:10.1016/j.ijleo.2020.164682.
- [5] C. Suresh, H. Nagabhushana, R.B. Basavaraj, G.P. Darshan, D. Kavyashree, B. Daruka

- Prasad, S.C. Sharma, R. Vanithamani, SiO₂@LaOF:Eu³⁺ core-shell functional nanomaterials for sensitive visualization of latent fingerprints and WLED applications, *J. Colloid Interface Sci.* 518 (2018) 200–215. doi:10.1016/j.jcis.2018.01.093.
- [6] G. Kriek, A. Sarakovskis, M. Springis, Upconversion luminescence of Er³⁺/Yb³⁺ and their role in the stabilization of cubic NaLaF₄ nanocrystals in transparent oxyfluoride glass ceramics, *J. Non. Cryst. Solids.* 481 (2018) 335–343. doi:10.1016/j.jnoncrysol.2017.11.016.
- [7] M. Ding, D. Chen, Lanthanide Ions Doped Upconversion Nanomaterials: Synthesis, Surface Engineering, and Application in Drug Delivery, Elsevier Inc., 2016. doi:10.1016/B978-0-323-47347-7.00009-4.
- [8] E. He, M. Zhang, H. Zheng, Y. Qin, B. Guan, H. Liu, M. Guo, Infrared to visible upconversion emissions of La_{1-0.02-x}Er_{0.02}Yb_xO_F nanorods, *Opt. Mater. (Amst).* 33 (2011) 275–279. doi:10.1016/j.optmat.2010.08.027.
- [9] Y.D. Eagleman, E. Bourret-Courchesne, S.E. Derenzo, Room-temperature scintillation properties of cerium-doped REOX (RE=Y, La, Gd, and Lu; X=F, Cl, Br, and I), *J. Lumin.* 131 (2011) 669–675. doi:10.1016/j.jlumin.2010.11.013.
- [10] C. Suresh, H. Nagabhushana, G.P. Darshan, R.B. Basavaraj, B. Daruka Prasad, S.C. Sharma, M.K. Sateesh, J.P. Shabaaz Begum, Lanthanum oxyfluoride nanostructures prepared by modified sonochemical method and their use in the fields of optoelectronics and biotechnology, *Arab. J. Chem.* 11 (2018) 196–213. doi:10.1016/j.arabjc.2017.03.006.
- [11] C. Suresh, Y.S. Vidya, H. Nagabhushana, K.S. Anantharaju, M. Venkataravanappa, K. Umeshareddy, Centella asiatica mediated solution combustion synthesis of a novel Pr³⁺ doped Lanthanum Oxyfluoride for display and visualization of latent fingerprints and

- anticounterfeiting applications, *J. Sci. Adv. Mater. Devices.* 6 (2021) 75–83. doi:10.1016/j.jsamd.2020.11.001.
- [12] N. Rakov, S.A. Vieira, Q.P.S. Silva, G.S. Maciel, Facile fabrication of Eu³⁺-doped lanthanum oxyfluoride powders by combustion processes and temperature analysis of its fluorescence for thermal sensor application, *Sensors Actuators, B Chem.* 209 (2015) 407–412. doi:10.1016/j.snb.2014.11.119.
- [13] Q. Xie, Y. Wang, B. Pan, H. Wang, W. Su, X. Wang, A novel photocatalyst LaOF: Facile fabrication and photocatalytic hydrogen production, *Catal. Commun.* 27 (2012) 21–25. doi:10.1016/j.catcom.2012.06.019.
- [14] C. Suresh, H. Nagabhushana, G.P. Darshan, R.B. Basavaraj, S.C. Sharma, D. V. Sunitha, B. Daruka Prasad, Positron annihilation spectroscopy and photoluminescence investigation of LaOF:Tb³⁺ nanophosphor fabricated via ultrasound assisted sonochemical route, *Mater. Sci. Eng. B Solid-State Mater. Adv. Technol.* 224 (2017) 28–39. doi:10.1016/j.mseb.2017.07.001.
- [15] W. Noh, S. Park, Synthesis and distinct up-converting behaviors of Er³⁺, Yb³⁺ doped LaOF and LaO_{0.65}F_{1.7} phosphors, *Opt. Mater. (Amst).* 66 (2017) 589–594. doi:10.1016/j.optmat.2017.02.057.
- [16] G. Cagnetta, Q. Zhang, J. Huang, M. Lu, B. Wang, Y. Wang, S. Deng, G. Yu, Mechanochemical destruction of perfluorinated pollutants and mechanosynthesis of lanthanum oxyfluoride: A Waste-to-Materials process, *Chem. Eng. J.* 316 (2017) 1078–1090. doi:10.1016/j.cej.2017.02.050.
- [17] N. Rakov, S.A. Vieira, R.B. Guimarães, G.S. Maciel, Investigation of Eu³⁺ luminescence enhancement in LaOF powders codoped with Tb³⁺ and prepared by combustion synthesis,

- J. Alloys Compd. 618 (2015) 127–131. doi:10.1016/j.jallcom.2014.08.140.
- [18] R. Li, G. Yu, Y. Liang, N. Zhang, Y. Liu, S. Gan, Morphology-controllable synthesis of LaOF: Ln³⁺ (Ln=Eu, Tb) crystals with multicolor luminescence properties, J. Colloid Interface Sci. 460 (2015) 273–280. doi:10.1016/j.jcis.2015.09.001.
- [19] D.C. Woo, M.H. Lee, W.S. Jung, Synthesis and characterization of rhombohedral- and tetragonal-lanthanum oxyfluoride powders, Ceram. Int. 39 (2013) 1533–1538. doi:10.1016/j.ceramint.2012.07.103.
- [20] T. Grzyb, M. Węclawiak, T. Pędziński, S. Lis, Synthesis, spectroscopic and structural studies on YOF, LaOF and GdOF nanocrystals doped with Eu³⁺, synthesized via stearic acid method, Opt. Mater. (Amst). 35 (2013) 2226–2233. doi:10.1016/j.optmat.2013.06.007.
- [21] Y. Luo, Z. Xia, L. Liao, Phase formation evolution and upconversion luminescence properties of LaOF:Yb³⁺/Er³⁺ prepared via a two-step reaction, Ceram. Int. 38 (2012) 6907–6910. doi:10.1016/j.ceramint.2012.05.005.
- [22] S.E. Dutton, D. Hirai, R.J. Cava, Low temperature synthesis of LnOF rare-earth oxyfluorides through reaction of the oxides with PTFE, Mater. Res. Bull. 47 (2012) 714–718. doi:10.1016/j.materresbull.2011.12.014.
- [23] J. Tauc, R. Grigorovici, A. Vancu, Optical Properties and Electronic Structure of Amorphous Germanium, Phys. Status Solidi. (1966). doi:10.1002/pssb.19660150224.
- [24] V. Kumar, J.K. Singh, Model for calculating the refractive index of different materials, Indian J. Pure Appl. Phys. (2010).
- [25] G.H. Dieke, H.M. Crosswhite, B. Dunn, Emission Spectra of the Doubly and Triply Ionized Rare Earths*, J. Opt. Soc. Am. 51 (1961) 820. doi:10.1364/josa.51.000820.